HOKKAIDO UNIVERSITY

Title	Plastic Deformation Simulation of REBCO Tapes Using Particle Methods
Author(s)	Mato, Takanobu; Noguchi, So
Citation	IEEE transactions on applied superconductivity, 32(6), 8400705 https://doi.org/10.1109/TASC.2022.3185568
Issue Date	2022-09
Doc URL	https://hdl.handle.net/2115/86749
Rights	© 2022 IEEE. Personal use of this material is permitted. Permission from IEEE must be obtained for all other uses, in any current or future media, including reprinting/republishing this material for advertising or promotional purposes, creating new collective works, for resale or redistribution to servers or lists, or reuse of any copyrighted component of this work in other works.
Type	journal article
File Information	MT_Paper_FINAL_VERSION_Takanobu_Mato.pdf

Plastic Deformation Simulation of REBCO Tapes Using Particle Methods

Takanobu Mato and So Noguchi, *Member, IEEE*

Abstract—Ultra-high field superconducting magnets are facing a mechanical degradation problem. On 2017, a world-record high DC magnetic field of 45.5 T was generated by insert no-insulation (NI) Rare-Earth Barium Copper Oxide (REBCO) pancake coils (14.4 T), called "LBC3", and an outsert resistive magnet (31.1 T). Although the experiment showed a high potential of the NI REBCO magnets for ultra-high field generation, the insert NI REBCO pancake coils and the REBCO tapes were plastically deformed. The critical current properties of damaged REBCO tapes were degraded although the Hastelloy substrate of REBCO tapes is stiff and it has a high yield point of approximately 1 GPa. However, the mechanisms of the damaging REBCO tapes are not clarified. Therefore, it is necessary to clarify the mechanical phenomenon of REBCO tapes.

In this paper, we model a REBCO tape with a smoothed particle hydrodynamics (SPH) method, which can represent plastic deformation. The SPH simulation is coupled with electromagnetic analysis with a partial element equivalent circuit (PEEC) model which we have previously developed. In the simulation, an external field, which linearly increases to 5 T and then decreases to 0 T, is applied to a short-length REBCO tape. The simulation results show that the REBCO tape largely deforms during the external field excitation and deexcitation.

Index Terms—mechanical simulation, particle method, plastic deformation, REBCO tape, screening current.

I. Introduction

THE performances of ultra-high field superconducting magnets have been drastically improving [1]–[4]. On 2017, a world-record high DC magnetic field of 45.5 T was generated with insert no-insulation (NI) Rare-Earth Barium Copper Oxide (REBCO) pancake coils (14.4 T), called "LBC3", and an outsert resistive magnet (31.1 T) [5]. After 45.5-T generation, the insert NI REBCO pancake coils were quenched, and plastic deformations of REBCO tapes were observed [6]. Since the Hastelloy substrate of REBCO tapes is stiff, whose yield point is 800 MPa[7], REBCO tapes have great mechanical properties together with high critical current density and critical magnetic field. NI REBCO pancake coils showed their potential to generate an ultra-high magnetic field beyond 30 T. However, REBCO tapes were plastically deformed and dam-

aged in several cases after high field generation; e.g., the LBC3 [5], [6], and the MIT 1.3-GHz NMR insert magnet [8]. The critical current (I_c) properties of the damaged REBCO tape were degraded. One of the possible reasons for I_c degradation is large unexpected deformation due to screening currents.

When an external field is applied to a REBCO tape, a screening current flows in the REBCO tape as shown in Fig. 1. A large magnetic force due to the screening current is generated on the edges of REBCO tape, and the REBCO tape would largely deform. A similar phenomenon would happen in REBCO windings. Although several methods for the mechanical stability improvements were proposed [9], [10], it is necessary to clarify the mechanical phenomenon of both REBCO tapes and windings towards further developments of ultra-high magnetic field magnets.

So far, some journal papers on mechanical simulation on REBCO magnets have been published [11]–[14]. In these papers, the finite element method (FEM) was employed as a mechanical simulation. However, the FEM cannot accurately simulate plastic deformations. Hence, we model REBCO tapes with a particle method for mechanical simulation in this paper. The particle method, particularly the Smoothed Particle Hydrodynamics (SPH) method, can represent plastic deformation of the material, such as the large deformation of REBCO tape. The simulated mechanical behaviors of REBCO tapes under large electromagnetic force are shown in this paper.

II. Simulation Methods

As the simulation methods, we coupled the electromagnetic simulation with plastic deformation simulation as shown in Fig. 2. A 3-D Partial Element Equivalent Circuit (PEEC) method is adopted for the electromagnetic simulation [15]. The PEEC method enables to simulate an accurate screening current with short computation time. A REBCO tape is modeled with a number of inductances L and REBCO resistances R_{re}. The nonlinear electrical properties of the REBCO layer
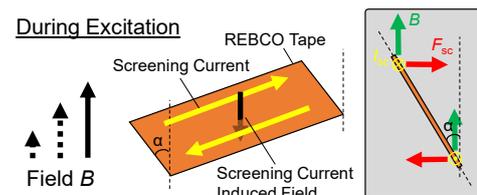
T. Mato and S. Noguchi are with the Graduate School of Information Science and Technology, Hokkaido University, Sapporo 060-0814, Japan. (e-mail: mato@em.ist.hokudai.ac.jp, noguchi@ssi.ist.hokudai.ac.jp).

Color versions of one or more of the figures in this paper are available online at http://ieeexplore.ieee.org.

Digital Object Identifier will be inserted here upon acceptance.

Fig. 1. Schematic explanation of damaging REBCO tape during external field excitation.

are considered with the power index model [16] considering the J_c-B-θ characteristics.

A Smoothed Particle Hydrodynamics (SPH) method is used for the mechanical simulation [17]. The SPH method is one of the meshfree methods having attention. The SPH method features fast computation and easy implementation. The SPH method can accurately represent plastic deformation as well as the elastic deformation of the REBCO tape. In the SPH method, REBCO tapes are represented by a set of particles, which are governed by the continuity equations and the constitutive law as follows:

$$\frac{D\boldsymbol{v}}{Dt} = \nabla \cdot (-p\boldsymbol{I} + \boldsymbol{\tau}) + \boldsymbol{f}_{\text{mag}} \tag{1}$$

$$\frac{D\rho}{Dt} = -\rho \nabla \cdot \boldsymbol{v} \tag{2}$$

$$\dot{\boldsymbol{\tau}} = G\left(\dot{\boldsymbol{\varepsilon}} - \frac{1}{3}\text{tr}(\dot{\boldsymbol{\varepsilon}})\boldsymbol{I}\right) \tag{3}$$

where $\boldsymbol{v}$, p, $\boldsymbol{I}$, $\boldsymbol{\tau}$, ρ, $\boldsymbol{f}_{\text{ex}}$, G, and $\boldsymbol{\varepsilon}$ are, respectively, the velocity, the pressure, the identity matrix, the shear stress tensor, the density, the external force per unit volume, the shear modulus, and the strain tensor. The third equation (3) is the well-known Hook's law. First, the shear stress tensor is updated according to Hook's law (3). Here, the strain tensor is also updated by the following derivative:

$$\dot{\boldsymbol{\varepsilon}}^{ij} = \frac{1}{2}\left(\frac{\partial \boldsymbol{v}^i}{\partial t} + \frac{\partial \boldsymbol{v}^j}{\partial t}\right) \tag{4}$$

where $\boldsymbol{v}^i$ represents the ith component of the velocity. For the plastic deformation analysis, we modeled the REBCO tape as
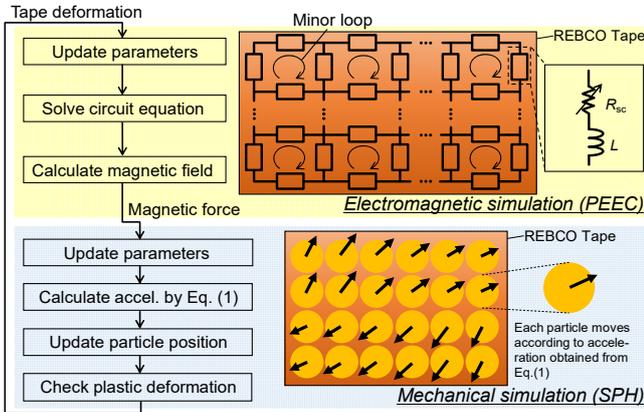

Fig. 2. Simulation flow of electromagnetic simulation code combined with mechanical simulation. A Partial Element Equivalent Circuit (PEEC) method and A Smoothed Hydrodynamics method are used.
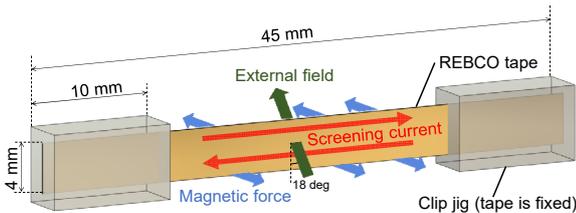

Fig. 3. REBCO tape deformation during field excitation process. Large magnetic force is applied to REBCO tape.

TABLE I
TAPE SPECIFICATIONS AND OPERATING CONDITIONS

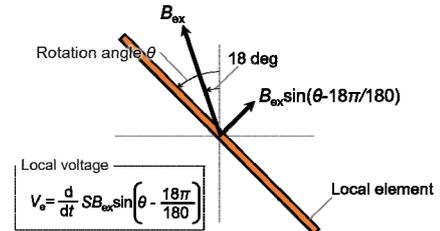| Parameters	Values
Tape length [mm]	45
Tape width [mm]	4.0
Tape thickness [μm]	50
Clip length [mm]	10
Mass density [kg/m³]	8890
Young's modulus [GPa]	182
Shear modulus [GPa]	69
Yield strength [MPa]	800
Operating temperature [K]	4.2
Critical current, s.f. @ 77 K [A]	120
n value	25
Field sweep rate [T/min.]	1.0

Fig. 4. Angles of REBCO tape and external field B_{ex}.

a perfectly plastic model. That is, when the von Mises stress exceeds a yield point, the shear tensor is scaled back to the yield point. The density change is computed with (2). The pressure is derived from the equation of state [18]. Then the velocity change is calculated according to (1). Finally, the particle positions are updated with the acceleration. The differential terms are computed with the weighted average of the physical values within the kernel radius. In this simulation, the quintic kernel is adopted [19]. Also, boundary techniques are not incorporated.

The magnetic forces obtained with the electromagnetic simulation are input as the external forces in (1). The deformation result is feedbacked to the electromagnetic simulation. That is, the REBCO tape rotation angle θ, shown in the Fig. 4, is transferred to the PEEC model to consider the induced voltage V_e on minor loops (shown in Fig. 2) according to Faraday's law:

$$V_e = \frac{\text{d}}{\text{d}t}SB_{\text{ex}}\sin\left(\theta - \frac{18}{180}\pi\right) \tag{5}$$

where S is the area of minor loops and B_{ex} is the external magnetic field. It is noted the rotation angle θ is the local average angle of each minor loop as shown in Fig. 2. The relation of the rotation angle θ and the magnetic field is also taken into account to specify the local critical current density.

III. SIMULATION METHOD AND RESULTS

The short-length REBCO tape whose ends are clipped, as shown in Fig. 3, is simulated under the conditions listed in Table I. An external field is applied with an angle of 18 degrees, and it is linearly ramped up to 5 T with 1.0 T/min. When the field reaches 5 T, the field immediately starts to decrease with -1.0 T/min. No enforced current flows in the REBCO tape.

The Young's modulus and the shear modulus are calculated from the composite rule with copper and Hastelloy. The yield point of the composite material is 800 MPa [7].

A. Magnetic force and deformation

Fig. 5 shows the cross-sectional view of the REBCO tape during external field excitation. The arrows represent the magnetic force vectors. At $t = 60$ s, a small deformation appears, and the tape slightly rotate due to positive torque. Since the screening currents are induced on both top and bottom edges, the REBCO tape rotates with torque. At $t = 120$ s, when the external field reaches 2 T, the screening currents are more induced, and the tape cross-section forms an S-shape. As the large shear forces work in the middle part of the REBCO tape, plastic deformation occurs. Consequently, a large deformation can be observed. When the time reaches 180 s, the magnetic force orientation turns opposite due to the opposite-directional induced current caused by deformation. At this time, the REBCO tape is subjected to the force that makes the deformation back. When the time passes 240 s, the tape deformation is close to the initial form; however, the large magnetic
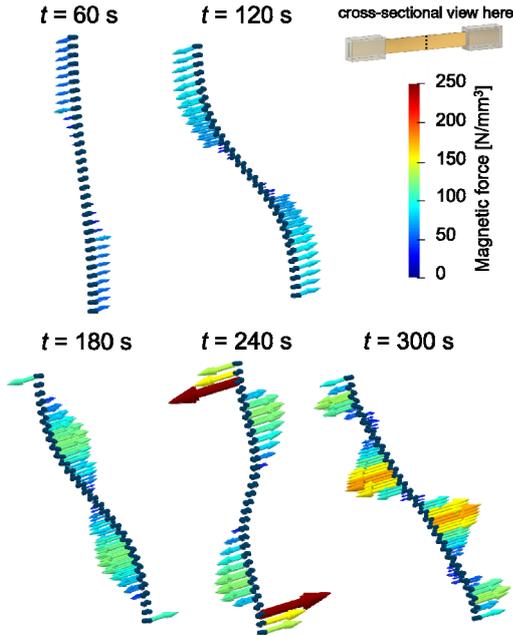

Fig. 5. REBCO tape deformation and magnetic force during field excitation process. Cross-sectional views are shown. Large magnetic force is applied to REBCO tape, and REBCO tape rotates.
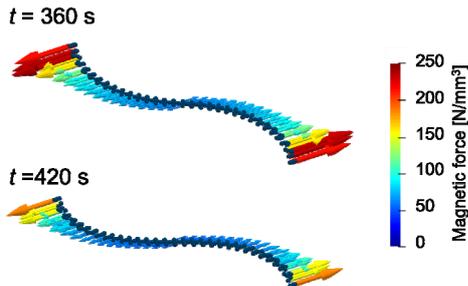

Fig. 6. REBCO tape deformation at 360 s and 420 s during demagnetization.

forces can be seen on the REBCO tape edges due to the induced current remaining in the tape edge. Thus, the REBCO tape rotates so as to be identical to the field orientation as shown at $t = 300$ s.

After the external field starts decreasing at 300 s (5 T), the tape deforms as shown in Fig. 6. The larger deformation is seen than that during the external field excitation. The mechanism is explained in the Fig. 7. In this case, the rotation angle of the REBCO tape is beyond 18 degrees at the start of the field demagnetization. The screening current is more induced in the same direction as that during field excitation. The magnetic force still works to rotate and expand the REBCO tape, and the REBCO tape rotates so that the rotation angle expands. The force direction and the current flowing direction do not change during the field decreasing, because the tape rotation angle keeps over 18 degrees which is the external field angle. The force intensity decreases with time, and the tape cross section eventually remains an S-shape due to the plastic deformation.

B. Stress distribution

Fig. 8(a) shows the von Mises stress distributions at $t = 60$, 120, and 180 s, and Fig. 8(b) is the enlargement view of the REBCO tape at the middle. The von Mises stress is a value used to determine whether the REBCO tape is in an elastic or plastic region. The von Mises stress σ_{Mises} is calculated from

$$\sigma_{\text{Mises}} = \sum_{i,j}^{x,y,z} \sqrt{\frac{3}{2} \tau^{ij} \tau^{ij}}. \tag{6}$$

Due to large magnetic forces, large stress occurs inside the REBCO tape. The stress concentration at the tape-clipping ends is observed at $t = 60$ s. The plastic region develops with time as shown at $t = 120$ and 180 s. Meanwhile, the plastic region inside the REBCO tape can be also seen in Fig. 8(b). Since the opposite forces acting on the upper and lower surfaces of the tape surface create a large shearing force, the tape experiences a tensile or compressive force at the middle of the REBCO tape. Thus, the von Mises stresses increase up to the
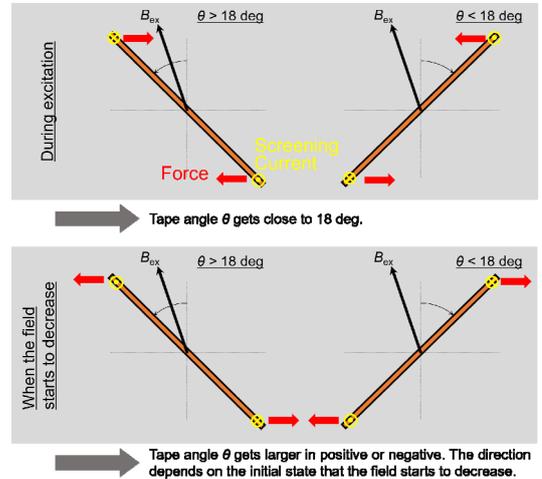

Fig.7. Mechanism of tape rotation angle during excitation or de-excitation.

yield point. The tape strains develop at the plastic regions.

The comparison between our proposed model and the elastic FEM-based model [20] is shown in Fig. 9. The REBCO tape is shown in the same scale. The FEM-based model does not consider plastic behavior deu to a used comercial software. In the FEM-based model, the large tension can be seen just outside the clipped portions because the plastic region is not considered. It causes the gentle curve. In the proposed model, which can deal with the plastic behavior, the tape moves entirely keeping a line, because the REBCO tape locally reaches the plastic region just at the outside of the clipped portions, and a large tension is not absent. The deformation between the proposed and FEM-based models looks similar; however, the stress behavior completely differs. After the stress of REBCO tape reaches the yield criterion, the results simulated with and without plastic property consideration are much different.

C. Current distribution

Next, we discuss the current distributions in the REBCO tape. Fig. 10 shows the current distributions during the external field excitation. The only left half of the tape is shown for symmetry. The screening current starts flowing along the top and bottom edges at the beginning of the excitation. When the current density reaches the critical current density, the current propagates into the inside of the tape. Thus, the current penetration develops, and the screening currents are widely distrib-

(a) Overall view

Stress concentration at edges

(b) Enlarged view

t = 60 s

Plastic region develops

t = 120 s

t = 180 s

0   200   400   600   800
von Mises stress [MPa]

(b) Enlarged view

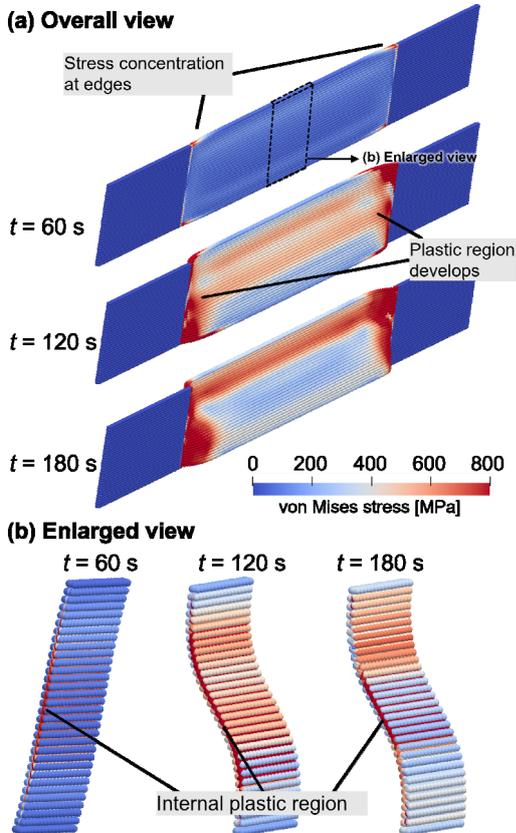t = 60 s t = 120 s t = 180 s

Internal plastic region

Fig. 8.   Von Mises stress distributions of REBCO tape. Tape ends near clipping reach to a yield point first. Tape central part also develops plastic region internally.
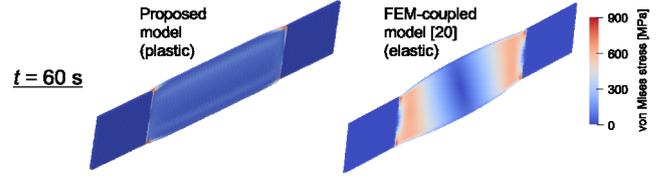

Proposed model (plastic)   FEM-coupled model [20] (elastic)

t = 60 s

900   600   300   0   von Mises stress [MPa]

Fig. 9.   Comparison between proposed model and FEM-coupled model [20].

t = 60 s

t = 120 s

t = 180 s

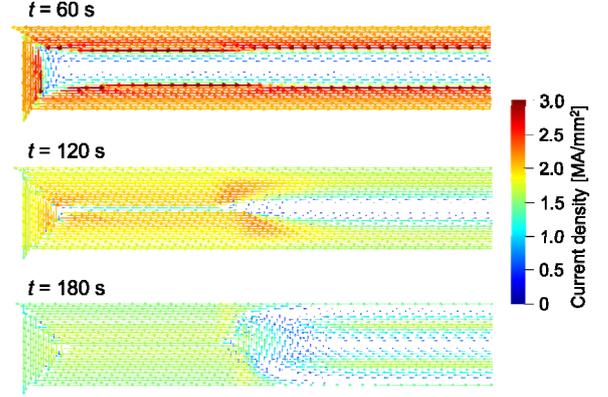3.0   2.5   2.0   1.5   1.0   0.5   0   Current density [MA/mm²]

Fig. 10.   Current distribution inside the REBCO tape. Screening currents decrease at the middle of the tape due to deformation.

uted at t = 60 s. Due to the screening current, the REBCO tape strains largely. Due to the deformation, the screening current decreases mainly at the middle of the tape at t = 120 s. When the field reaches 3 T (180 s), the complicated screening current distribution can be seen due to the deformation, and the intensity of the screening current is not so large. However, the large field is applied to the tape externally, the large magnetic force appears.

IV. CONCLUSION

In this paper, we simulated the mechanical behavior of a REBCO tape during external field excitation. We have developed the electromagnetic simulation code coupled with the mechanical simulation by a Smoothed Particle Hydrodynamics (SPH) method. This method enables to represent plastic deformation.

As the result, large deformation of the REBCO tape during external field excitation can be observed. This is due to a large magnetic force caused by screening currents. The plastic regions of REBCO tape are seen mainly near the clipping ends and the middle of REBCO tape. The deformation at these regions develops and results in large plastic deformation. Meanwhile, the screening current decreases due to the deformation, and the REBCO tape rotates so that the cross-section is aligned with the magnetic field direction.

The clear S-shape of the REBCO tape cross-section is observed due to the plastic deformation, which is not seen in the mechanical simulation by FEM analysis. In the near future, we will expand the simulation target from the REBCO tape to REBCO windings, and the deformation mechanism of the REBCO windings will be investigated.

REFERENCES

[1] P. C. Michael *et al.*, "Assembly and Test of a 3-Nested-Coil 800-MHz REBCO Insert (H800) for the MIT 1.3 GHz LTS/HTS NMR Magnet," *IEEE Trans. Appl. Supercond.*, vol. 29, no. 5, 2019, Art. no. 4300706.

[2] M. Niu, J. Xia, and H. Yong, "Numerical Analysis of The Electromechanical Behavior of High-Field REBCO Coils in All-Superconducting Magnets," *Supercond. Sci. Technol.*, vol. 34, no. 11, 2021, Art. no. 115005.

[3] B. Parkinson, "Design Considerations and Experimental Results for MRI Systems Using HTS Magnets," *Supercond. Sci. Technol.*, vol. 30, no. 1, 2016, Art. no. 014009.

[4] J. Liu, L. Wang, L. Qin, Q. Wang, and Y. Dai, "Design, Fabrication, and Test of A 12 T REBCO Insert for A 27 T All-Superconducting Magnet," *IEEE Trans. Appl. Supercond.*, vol. 30, no. 5, 2020, Art. no. 5203006.

[5] S. Hahn *et al.*, "45.5-Tesla Direct-Current Magnetic Field Generated with A High-Temperature Superconducting Magnet," *Nature*, vol. 570, pp. 496-499, 2019.

[6] X. Hu *et al.*, "Analyses of The Plastic Deformation of Coated Conductors Deconstructed from Ultra-High Field Test Coils," *Supercond. Sci. Technol.*, vol. 33, no. 9, 2020, Art. no. 095012.

[7] C. C. Clickner *et al.*, "Mechanical Properties of Pure Ni and Ni-alloy Substrate Materials for Y–Ba–Cu–O Coated Superconductors," *Cryogenics*, vol. 46, no. 6, pp. 432-438, 2006.

[8] D. Park, J. Bascuñán, Y. Li, W. Lee, Y. Choi, and Y. Iwasa, "Design Overview of the MIT 1.3-GHz LTS/HTS NMR Magnet with a New REBCO Insert," *IEEE Trans. Appl. Supercond.*, vol. 31, no. 5, 2021, Art. no. 4300206.

[9] T. Qu *et al.*, "Test of an 8.66-T REBCO Insert Coil with Overbanding Radial Build for a 1.3-GHz LTS/HTS NMR Magnet," *IEEE Trans. Appl. Supercond.*, vol. 27, no. 4, 2017, Art. no. 4600605.

[10] T. Mato, S. Hahn, and S. Noguchi, "Mechanical Damage Protection Method by Reducing Induced Current in NI REBCO Pancake Coils During Quench Propagation," *IEEE Trans. Appl. Supercond.*, vol. 31, no. 5, 2021, Art. no. 4602405.

[11] S. Takahashi *et al.*, "Hoop Stress Modification, Stress Hysteresis and Degradation of a REBCO Coil Due to the Screening Current Under External Magnetic Field Cycling," *IEEE Trans. Appl. Supercond.*, vol. 30, no. 4, 2020, Art. no. 4602607.

[12] H. Ueda, Y. Awazu, K. Tokunaga, and S. Kim, "Numerical Evaluation of The Deformation of REBCO Pancake Coil, Considering Winding Tension, Thermal Stress, And Screening-Current-Induced Stress," *Supercond. Sci. Technol.*, vol. 34, no. 2, 2021, Art. no. 024003.

[13] D. Kolb-Bond *et al.*, "Screening Current Rotation Effects: SCIF And Strain in REBCO Magnets," *Supercond. Sci. Technol.*, vol. 34, no. 9, 2021, Art. no. 095004.

[14] Y. Yan *et al.*, "Screening-Current-Induced Mechanical Strains in REBCO Insert Coils," Supercond. Sci. Technol., vol 34, no. 8, 2021, Art. no. 085012.

[15] S. Noguchi and H. Seungyong, "A Newly Developed Screening Current Simulation Method for REBCO Pancake Coils Based on Extension of PEEC Model," to be published on *Supercond. Sci. Technol*, 2021, DOI: 10.1088/1361-6668/ac5315.

[16] F. Trillaud, G. D. Santos, and G. G. Sotelo, "Essential Material Knowledge and Recent Model Developments for REBCO-Coated Conductors in Electric Power Systems," *Materials*, vol. 14, no. 8, 2021, Art. no. 1892.

[17] G. R. Liu and M. B. Liu, *Smoothed Particle Hydrodynamics: A Meshfree Particle Method*, Tho Tuck Link, Singapore: World Scientific Publishing, 2003.

[18] J. P. Gray, J. J. Monaghan, and R. P. Swift, "SPH elastic dynamics," *Comput. Methods Appl. Mech. Eng.*, vol. 190, no. 49, pp. 6641-6662, 2001.

[19] J. P. Morris, P. J. Fox, and Y. Zhu, "Modeling Low Reynolds Number Incompressible Flows Using SPH," *J. Comput. Phys.*, vol. 136, no. 1, pp. 214-226, 1997.

[20] K. Thomas, T. Mato, and S. Noguchi, "Screening current simulation of REBCO pancake coils considering coil deformation," presented at MT27, WED-PO2-718-10, Fukuoka, Nov. 2021.